

Robust Micro-positioning Control of a 2DOF Piezocantilever Based on an Extended-State LKF [☆]

J. Escareno^a, J. Abadie^b, E. Piat^b, M. Rakotondrabe^b

^a*XLIM Research Institute, UMR CNRS 7252, Limoges University, 16 Rue Atlantis, 87280 Limoges, France*

^b*FEMTO-ST Institute, University Bourgogne Franche-Comte, CNRS UMR6174, UFC, ENSMM, UTBM 24 rue Alain Savary, 25000 Besancon, France*

Abstract

This paper presents a control scheme regarding to improve the performances of a piezoelectric actuator (PEA) for precise positioning tasks. The piezoelectric actuator exhibits strong nonlinear disturbances for 1- and 2-DOF motion, i.e. input-dependent hysteresis, creep and cross-couplings. These unwanted phenomena undeniably compromise the final precision of the targeted tasks (micromanipulation) and therefore it should be conveniently considered during the controller synthesis. In this regard, the dynamic equation is also split into a nominal model and a uncertain model including parametric uncertainties. We propose to use simultaneously a the discrete linear extended-state linear Kalman filter (ES-LKF), to estimate the aforementioned disturbances and the velocity, and Lyapunov-based controller to guarantee asymptotic stability while meeting the actuator limits. The proposed strategy permits to perform accurate positioning, for regulation and trajectory-tracking tasks, without a prior knowledge of parametric and unmodeled uncertainties. Real-time experiments were carried out with circular trajectories to demonstrate the efficiency of the proposed approach.

Key words: Piezoelectric cantilever, extended-state linear Kalman filter, robust micro-positioning, disturbance estimation and compensation,

Email addresses: juan.escareno-castro@unilim.fr (J. Escareno), jabadie@femto-st.fr (J. Abadie), epiat@ens2m.fr (E. Piat), mrakoton@femto-st.fr (M. Rakotondrabe)

parametric and dynamic uncertainties, bounded-input controller.

1. Introduction

2 These last years, the advance of microrobotics has increasingly enhanced dif-
ferent applications. Particularly, in micromanipulation applications, technolo-
4 gies based on piezoelectric actuators represent a wide spectrum ranging from
walking actuators, multi-DOF positioning systems to manipulation (transport
6 and pick-and-place) of micro-sized objects. The advantageous performances
profile provided by piezoelectric actuators (PEAs), bandwidth and resolution,
8 is however degraded by static and dynamic disturbances (hysteresis and creep).
Such PEAs adverse behavior depends on both current and past inputs. Hystere-
10 sis arises either in static regime (constant inputs) or dynamic regime (fast-/slow-
time varying inputs). Furthermore, multi-DOF micropositioning applications
12 bring unwanted cross-couplings for both sequenced or simultaneous motions.

The control of PEAs has been addressed using feedforward and feedback
14 control approaches, or a combination of both. Feedforward-based schemes rely
on the accuracy of the PEA's model and thus its inverse is able to compen-
16 sate hysteresis reaching desired displacements. In the feedforward control of
PEAs, several approaches are available to model and then to compensate for
18 the hysteresis: the Preisach [1][2][3], the Prandtl-Ishlinskii [4][5][5][6][7] and the
Bouc-Wen approaches [8][9]. In the two formers, a complex hysteresis is mod-
20 eled by the sum of many basic hysteresis (hysterons). Both approaches can be
very accurate with the use of a high number of elementary hysteresis, which
22 represents a computational burden implementation. Alternatively, the Bouc-
Wen model of hysteresis, has an interesting simplicity and is able to represent
24 a large class of hysteresis. Although the low cost and the high packageability
(no sensors required) of the used feedforward control approaches, their main
26 limitation is the lack of robustness face to model uncertainties and to external
disturbances.

28 On the other hand, feedback control has been used to deal with the motion

control of PEAs. In this case, the controller's performances will be as good as
30 the quality of the measurements and/or the estimation of the system's states,
which in practice are noisy and/or missing (e.g. only position measurement is
32 available). Two control applicative categories might be distinguished based on
the control operational regime:

- 34 • *Regulation Task*

In this regime, hysteresis, creep and couplings (multi-DOF PEAs) are
36 considered as a constant disturbance introducing a static error. Thus,
classical PID or event intelligent adaptive schemes can fulfill the control
38 objective[10][11].

- *Trajectory-tracking Task*

40 The aforementioned parasitic disturbances become dynamic. Therefore,
robust control schemes are required to overcome significant uncertainties.
42 Recent works encompass sliding-mode control (SMC), SMC+adaptive and
 H_∞ schemes. Such controllers are able to reject the effect of the afore-
44 mentioned disturbances[12][13][14][15][16].

State observers, either deterministic or stochastic, represent an interesting al-
46 ternative for both operation profiles, not only to estimate missing states (e.g.
velocity) and/or to improve state(s) measurement(s) (e.g. filtering[17]) but also
48 to estimate unknown inputs (1DOF unknown input observers [18],[19]) In this
case, we have accomplished effective tracking of simultaneous time-varying tra-
50 jectories (while rejecting inherent parasitic and dynamic uncertainties) having
only position measurement while velocity is estimated from the ES-LKF. This
52 reinforce and validates the proposed estimation and bounded-controller archi-
tectures. We are interested on (at micro/nano level) measurement resolution,
54 displacement, and the accuracy of them and eventually their dynamics (see [20]).
For this reason, it is important to have reliable sensory systems featuring such
56 performance.

The present paper addresses a multi-DOF piezoelectric micro-positioning
58 actuator devoted to dexterous micro-positioning tasks. The worst-case sce-

nario corresponds to piezocantilever's simultaneous motion tracking a time-
60 varying trajectory. Besides parasitic disturbances, input-dependent hysteresis
and creep, input-interconnection couplings also degrades the positioning per-
62 formance. From experimental observations on specific off-the-shelf piezocan-
tilevers, we have witnessed that the parameters change during repeated test
64 solicitation affecting the closed-loop effectiveness. Therefore, to apply the afore-
mentioned control schemes for extensive trials requires a prior-to-trial identifi-
66 cation phase. Alternatively we have proposed to split the dynamic model into a
nominal model, that features initial identification parameters, and an uncertain
68 parameters variations denoting the parametric disturbance. Both uncertainty
terms, dynamic and parametric, are condensed into a overall lumped disturbance
70 which will be further estimated. In order to overcome such evoked issues, we
proposed and implemented in real-time a generalized disturbance compensation
72 scheme based on an extended-state linear Kalman filter (ES-LKF) combined
with a bounded-input controller. Unlike the previous works cited above, the
74 actuator limits are considered within stability analysis which lies within the
Backstepping technique. The asymptotically stability of the closed-loop system
76 needs to be explicitly proven while experimental controllers are used due the
nonlinear nature of the saturation of the actuator(s). Furthermore, for these
78 kind of applications, if the voltage amplitude is too high, there is a risk of
depolarization of the material leading to a loss of the piezoelectric properties.
80 Consequently, overvoltages due to an excessive solicitation on the piezoelectric
actuator to effectuate rapid responses (large bandwidth) or large courses may
82 destroy the latter. Therefore, in this paper we design a controller that meets
the real actuator's limits while providing asymptotic stability analysis. We have
84 conducted an experimental stage to evaluate the trajectory tracking of the of
the piezocantilever for a two-dimensional time-parametrized references trajecto-
86 ries, whose effectiveness is validated not only for the disturbance compensations
(effective estimation) but also meeting the saturation limits of the controller.
88 Furthermore, trajectory tracking of second order systems, as PEAs, requires the
knowledge of both states.

90 The paper is organized as follows: the description and model of the piezo-
 cantilever is presented in section-2. In section-3 the characteristics of the exper-
 92 imental setup are described. In section-4 is described the LKF-based estimation
 algorithm as well as the closed-loop compensation scheme. Numerical and Ex-
 94 perimental results are presented in section 5 and 6, respectively. Finally, the
 conclusions and perspectives are given in section-7.

96 2. Dynamic Modeling of the Piezocantilever

The actual paper considers as reference model for the piezocantilever the
 98 Bouc-Wen model of hysteresis, which corresponds to a cascade structure fea-
 turing a static hysteresis model plus a second order linear dynamic system (see
 100 Fig. 1). Such model stands out for its simplicity regarding computation and
 implementation. Another aspect is the compatibility of the the Bouc-Wen model
 102 for controllers synthesis [8][9].

The nonlinear equations which model the behavior of the multi-DOFs piezo-
 104 cantilever are written as

$$\begin{cases} a_i \ddot{\delta}_i + b_i \dot{\delta}_i + \delta_i = d_{pi} u_i - \mathcal{H}_i \\ \dot{\mathcal{H}}_i = d_{pi} A_{bwi} \dot{u}_i - B_{bwi} |\dot{u}_i| h_i - C_{bwi} \dot{u}_i |h_i| \end{cases} \quad (1)$$

where δ_i is the motion of the i -axis, $i \in \{y, z\}$ correspond to the bi-axial dis-
 106 placement, A_{bwi} , B_{bwi} and C_{bwi} are coefficients determining the hysteresis shape
 and amplitude and d_{pi} is a positive coefficient that defines the magnitude deflec-
 108 tion, while h_i represents the hysteresis internal state. The dynamic parameters

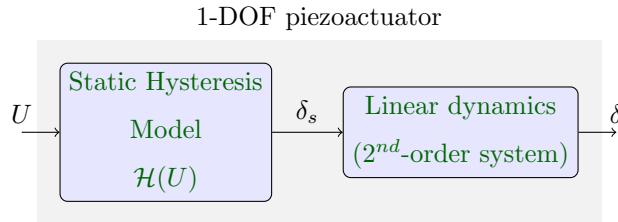


Figure 1: Hammerstein Model of a 1-DOF Piezocantilever

are denoted by a_i and b_i , which are obtained through an identification process.
 110 In our case, these parameters are set to a typical (or average) specifications of
 the piezocantilever.

112 *2.1. Model Extension*

Single-axis positioning evolves in presence of hysteresis \mathcal{H}_i and creep \mathcal{C}_i ,
 whereas, a bi-axial motion introduces a novel disturbances, generated by a dy-
 namic input-interconnection couplings. The coupling effects are depicted (see
 Fig. 2). Such adverse couplings increase during simultaneous 2D operations, i.e.
 tracking a time-varying circular trajectories. From the latter we can regroup
 creep (for details see [4]) cross couplings into a **generalized disturbance** Θ_i , i.e.

$$\Theta_i = -\mathcal{H}_i + \mathcal{C}_i + \mathcal{I}_i, \quad (2)$$

which allows to rewrite the nonlinear model (Equ. 1) as

$$a_i \ddot{\delta}_i + b_i \dot{\delta}_i + \delta_i = d_{pi} u_i + \Theta_i \quad (3)$$

where \mathcal{C}_i the creep terms, \mathcal{I}_i the interconnection disturbances (couplings). More-
 over, in some cases the accuracy of the coefficients of the dynamic equation

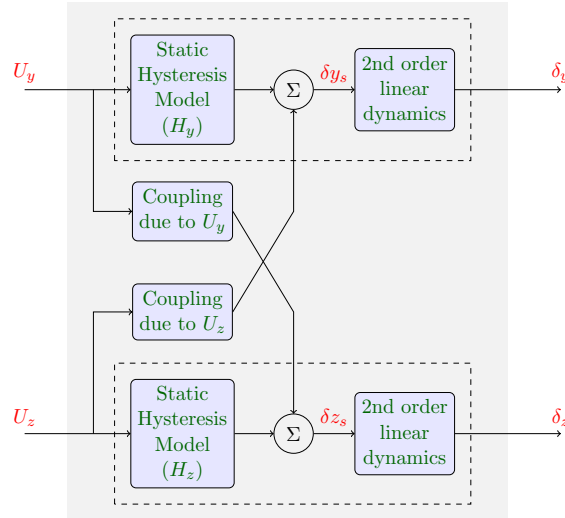


Figure 2: Block scheme of coupling's structure

(Equ. 3) varies in function of the identification process quality. Then, (Equ. 3) is rewritten as

$$\underbrace{(a_{N_i} + \Delta_{a_i})}_{a_i} \ddot{\delta}_i + \underbrace{(b_{N_i} + \Delta_{b_i})}_{b_i} \dot{\delta}_i + \underbrace{(c_{N_i} + \Delta_{c_i})}_{c_i} \delta_i = d_{pi} u_i + \Theta_i, \quad (4)$$

where $(\cdot)_{N_i}$ stand for the nominal/characteristic/initial values of the model, $\Delta_{(\cdot)_i}$ the parametric uncertainties. From the latter structure it is possible to include such parametric uncertainties into a lumped disturbance Θ_i reducing the system (Equ. 4) to

$$a_{N_i} \ddot{\delta}_i + b_{N_i} \dot{\delta}_i + c_{N_i} \delta_i = d_{pi} u_i + \Theta_i \quad (5)$$

with

$$\Theta_i = \underbrace{-\mathcal{H}_i + \mathcal{C}_i + \mathcal{I}_i}_{\text{parasitic nonlinearities}} - \underbrace{(\Delta_{a_i} \ddot{\delta}_i + \Delta_{b_i} \dot{\delta}_i + \Delta_{c_i} \delta_i)}_{\text{parametric uncertainties}} \quad (6)$$

3. Experimental Setup Description

114 The experimental positioning system features a 2DOF piezocantilever which
 evolves along the y and z axes. This actuator is designed with 36 piezo-electric
 116 layers to work at low input voltage. The total dimensions of the active part
 are $25 \times 1 \times 1$ mm³. This cantilever is controlled by two inputs U_y and U_z that
 118 are varying in the range of ± 20 volts. The first extremity of the cantilever is
 clamped while the other moves within the 2D y - z plane based on the input U_i
 120 with $i \in \{y, z\}$ (see Fig. 3).

3.1. Model Identification

122 The parameters corresponding to the coefficients of the dynamic equation
 (Equ.1) of the piezocantilever have been identified using the ARMAX approach
 124 (Autoregressive-moving-average model with exogenous inputs) with an experi-
 mental 10 Volts step response applied to the piezocantilever (see Tab. 1). For
 126 the sake of comprehension Fig. 5 illustrate the signals used for the identification
 process for the y -axis and its effect on the z -axis.

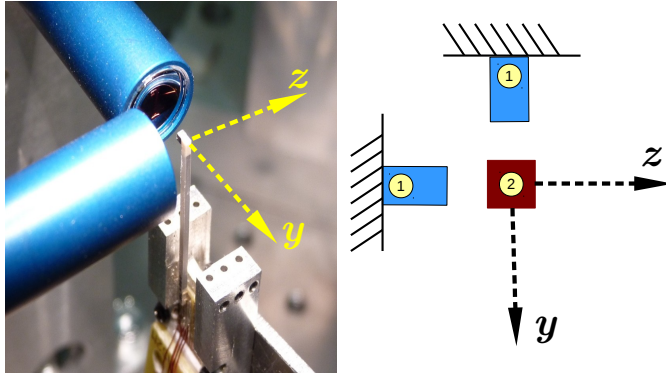


Figure 3: Experimental setup is composed of two cofocal sensors arranged orthogonally (1) and a piezoelectric cantilever (2)

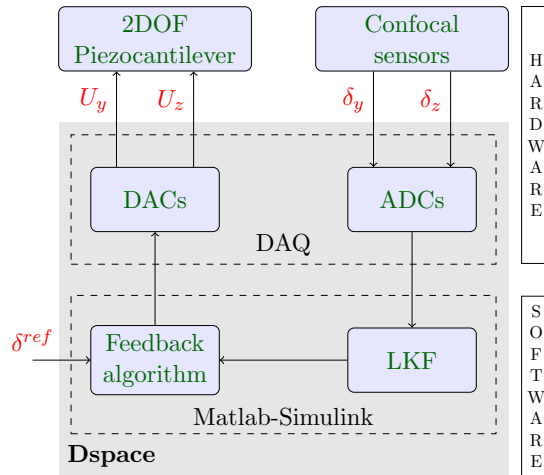


Figure 4: Experimental architecture

128 The cantilever displacement in the 2D yz -plane is given by δ_i , with $i \in \{y, z\}$.
 The measurement of δ_i is acquired by two external confocal sensors orthogonally
 130 arranged aiming at the the piezocantilever's tip (see Fig. 3).

4. Estimation and Control Strategy

A discrete linear Kalman filter (LKF) is designed and implemented in real-time to estimate the static and dynamic disturbances for a two-dimensional

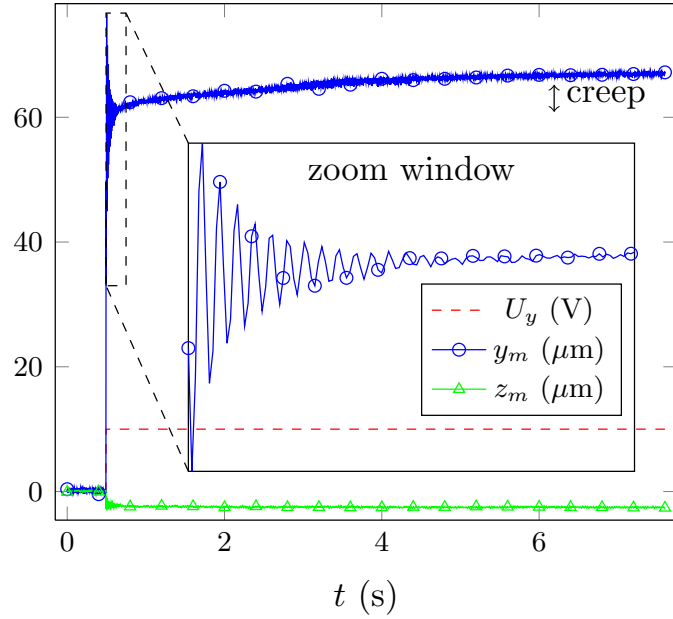


Figure 5: Piezocantilever step response to a 10V step input U_y ($U_z = 0$)

Parameter	value	Parameter	value
(y -axis)		(z -axis)	
a_{N_y}	4.4209×10^{-9}	a_{N_z}	3.5125×10^{-9}
b_{N_y}	3.7378×10^{-6}	b_{N_z}	2.9062×10^{-5}
d_{p_y}	5.13	d_{p_z}	3.702

Table 1: Dynamic parameters of the piezocantilever.

micro-positioning task of the piezocantilever. The Linear Kalman Filter (LKF) is derived from a 2^{nd} -order continuous state-space system

$$\begin{cases} \dot{x}(t) = Ax(t) + Bu(t) + \mathcal{M}\omega(t) & \rightarrow \text{process} \\ y(t) = Cx(t) + \nu(t) & \rightarrow \text{sensor(s)} \end{cases} \quad (7)$$

132 where the state vector $x = (\delta_i, \dot{\delta}_i)^T$. This model considers the following hypothesis:

134 **H1.** The pair AC verifies the observability property

H2. The terms $\omega(t) = (\omega^{\delta_i}, \dot{\omega}^{\delta_i})^T$ and $\nu(t) = (\nu^{\delta_i}, \dot{\nu}^{\delta_i})^T$ stand for a white Gaussian random process respectively and represent the uncertainties in the process and outputs (sensors). Such terms verify

$$E[\omega(t)] = 0 \text{ and } E[\nu(t)] = 0 \quad (8)$$

with constant power spectral density (PSD) $W(t)$ and $V(t)$ respectively.

The covariance matrix of the model

$$Q = E[\omega(t)\omega(t)^T] = \text{diag}[\sigma^2(\omega^{\delta_i}), \sigma^2(\dot{\omega}^{\delta_i})] \quad (9)$$

The sensor covariance matrix

$$R = E[\nu(t)\nu(t)^T] = \text{diag}[\sigma^2(\nu^{\delta_i}), \sigma^2(\dot{\nu}^{\delta_i})] \quad (10)$$

It is also assumed that both stochastic processes are not correlated, i.e.

$$E[\omega(t)\nu(t)^T] = 0 \quad (11)$$

136 4.1. Disturbance Estimation Based on ES-LKF

Let us recall the piezocantilever model given by [Equ. 5](#)

$$a_{N_i}\ddot{\delta}_i + b_{N_i}\dot{\delta}_i + c_{N_i}\delta_i = d_{pi}u_i + \Theta_i \quad (12)$$

This model corresponds to two scalar disturbed systems defining the motion behavior along y and z axes (see [Fig. 6](#)). This model may be rewritten into the state-space representation

$$\begin{aligned} \dot{x} &= Ax + Bu + Pd \\ y &= Cx \end{aligned} \quad (13)$$

The positions δ_i are provided by the confocal chromatic sensors and $d = \Theta_i$ corresponds to the dual-axis disturbance. The velocity is obtained via the estimation provided by the LKF. The matrices of the system ([Equ. 13](#)) are given

by:

$$A = \begin{pmatrix} 0 & 1 \\ -\frac{c_i}{a_i} & -\frac{b_i}{a_i} \end{pmatrix} B = \begin{pmatrix} 0 \\ \frac{d_{pi}}{a_i} \end{pmatrix} P = \begin{pmatrix} 0 \\ \frac{1}{a_i} \end{pmatrix} C = \begin{pmatrix} 1 & 0 \end{pmatrix} \quad (14)$$

It is assumed that no prior information about the disturbance is available. However, we consider that the disturbance has a slow time-varying dynamics that can be modeled by a random walk process

$$\dot{\Theta}_i = \omega^{\Theta_i}, \quad (15)$$

where $\omega^e(t) = (\omega^{\delta_i}, \omega^{\dot{\delta}_i}, \omega^{\Theta_i})^T$. The latter assumption allows us to introduce an extended state-space vector:

$$x^e = (\delta_i, \dot{\delta}_i, \Theta_i)^T \quad (16)$$

and its associated extended-state model describing the dynamics is obtained from (Equ. 15) in which the unknown input disturbance Θ_i is incorporated in the transition matrix:

$$\dot{x}^e = \mathcal{A}x^e + \mathcal{B}u + \mathcal{M}\omega^e \quad (17)$$

$$y = \mathcal{C}x^e + \nu \quad (18)$$

with

$$\mathcal{A} = \begin{pmatrix} 0 & 1 & 0 \\ -\frac{c_i}{a_i} & -\frac{b_i}{a_i} & \frac{1}{a_i} \\ 0 & 0 & 0 \end{pmatrix} \quad \mathcal{B} = \begin{pmatrix} 0 \\ \frac{d_{pi}}{a_i} \\ 0 \end{pmatrix} \quad (19)$$

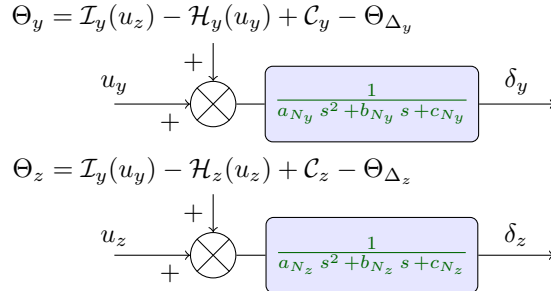


Figure 6: Simplified disturbed model

$$\mathcal{M} = \begin{pmatrix} 1 & 0 & 0 \\ 0 & 1 & 0 \\ 0 & 0 & 1 \end{pmatrix} \quad \mathcal{C} = \begin{pmatrix} 1 & 0 & 0 \end{pmatrix} \quad (20)$$

140 The continuous-time model (Equ. 17) can be discretized with sampling time T_s and considering a zero-order hold (zoh) yield

$$x_{k+1}^e = \mathcal{A}_k x_k^e + \mathcal{B}_k u_k + \omega_k \quad (21)$$

$$y_k = \mathcal{C}_k x_k^e + \nu_k \quad (22)$$

142 with

$$x_k^e = (\delta_{i_k}, \dot{\delta}_{i_k}, \Theta_{i_k})^T \quad (23)$$

$$\mathcal{A}_k = e^{\mathcal{A}T_s} \quad (24)$$

$$\mathcal{B}_k = \left(\int_0^{T_s} e^{\mathcal{A}T_s} \right) \mathcal{B} \quad (25)$$

$$\omega_k^e = (\omega_k^{\delta_i}, \omega_k^{\dot{\delta}_i}, \omega_k^{\Theta_i})^T \quad (26)$$

$$\nu_k^e = \nu_k^{\delta_i} \quad (27)$$

where ω_k and ν_k are discrete-time band-limited white gaussian random process with zero-mean characterizing uncertainties on the model (unmodeled dynamics and parametric uncertainties) and measurement (noisy sensors) equations, respectively. The model uncertainties discrete covariance matrix Q_k is:

$$Q_k = E \left[\omega_k^e \omega_k^{eT} \right] = \int_0^{T_s} e^{\mathcal{A}t} \mathcal{M} Q \mathcal{M}^T e^{\mathcal{A}^T t} dt \quad (28)$$

where the continuous covariance matrix stands for

$$Q = \text{diag}[\sigma^2(\omega_k^{\delta_i}), \sigma^2(\omega_k^{\dot{\delta}_i}), \sigma^2(\omega_k^{\Theta_i})] \quad (29)$$

The algorithm that computes the estimate (including the disturbance Θ_i) of the state vector x_k^e is initialized as follows:

- The piezocantilever-based micro-positioning system is in the equilibrium state

$$x_{k_0}^e = (0, 0, 0)^T \quad (30)$$

- The initial covariance matrix P_0 is considered as

$$P_0 = \text{diag} \left[\sigma^2(\delta_{i_0}), \sigma^2(\dot{\delta}_{i_0}), \sigma^2(\Theta_{i_0}) \right] \quad (31)$$

The corresponding LKF recursive algorithm features a prediction-estimation structure and is provided next

Prediction stage

$$\hat{x}_{est_k} = \mathcal{A}_k \hat{x}_{est_k} + \mathcal{B}_k u_k$$

$$P_{pred_k} = \mathcal{A}_k P_{est_k} \mathcal{A}_k^T + Q$$

$$K_k = P_{pred_k} \mathcal{C}_k^T (\mathcal{C}_k P_{pred_k} \mathcal{C}_k^T + R)^{-1}$$

Estimation stage

y_k = measurement vector

$$\hat{x}_{est_k} = \hat{x}_{pred_k} + K_k (y_k - \mathcal{C}_k \hat{x}_{pred_k})$$

$$P_{est_k} = (I - K_k \mathcal{C}_k) P_{pred_k} (I - K_k \mathcal{C}_k)^T$$

where K_k denotes the Kalman filter gain, and I is the identity matrix. The estimated vector state generated by the LKF is written:

$$\hat{x}_k^e = (\hat{\delta}_{i_k}, \dot{\hat{\delta}}_{i_k}, \hat{\Theta}_{i_k})^T \quad (32)$$

For the actual work it was considered

$$\hat{\Theta}_{i_k} = \mathcal{C}_d \hat{x}_k^e \quad (33)$$

with $\mathcal{C}_d = (0, 0, 1)^T$

146 4.2. Bounded-input Controller Design

Assuming the knowledge of the disturbance $\hat{\Theta}_{i_k}$, the goal consists in driving
 148 the equilibrium point of the actual piezoactuator through a controller whose
 asymptotic stability is demonstrated, but also a controller that meets the ac-
 150 tuator's limits (saturation). To this end, the Backstepping technique provides
 an appropriate framework to construct the controller since the aforementioned

152 dynamic model (Equ. 12) features a cascade form suitable to apply such control technique.

Let us remind the dynamic model by assuming that the voltage $u(t)$ is within the limitation:

$$\ddot{\delta} = \frac{d_p}{a} u - \frac{b}{a} \dot{\delta} - \frac{1}{a} \delta + \Theta \quad (34)$$

Where we have dropped the subscript i and N to avoid notation abuse. Since we are concerned on solving the trajectory tracking problem, the latter dynamic model is rewritten in terms of the error ξ . To do so, the control input must contain the reference dynamic $\ddot{\delta}^d$. Thus, the control input is written

$$u = \frac{a}{d_p} \left[u^* + \ddot{\delta}^d + \tanh \left(\frac{b}{a} \dot{\delta} + \frac{1}{a} \delta \right) \right] \quad (35)$$

where u^* will be designed later. Introducing (Equ. 35) in (Equ. 34) leads to cancel out the nominal dynamics, after an arbitrary time t_1 , since the piezocantilever features a stable behavior, i.e.

$$\lim_{t \rightarrow t_1} \tanh \left(\frac{b}{a} \dot{\delta} + \frac{1}{a} \delta \right) = \frac{b}{a} \dot{\delta} + \frac{1}{a} \delta \quad (36)$$

Through (Equ. 35) it is possible to perform a coordinates change allowing to rewrite the system in terms of the error.

$$\ddot{\xi} = \ddot{\delta} - \ddot{\delta}^d = u^* + \Theta \quad (37)$$

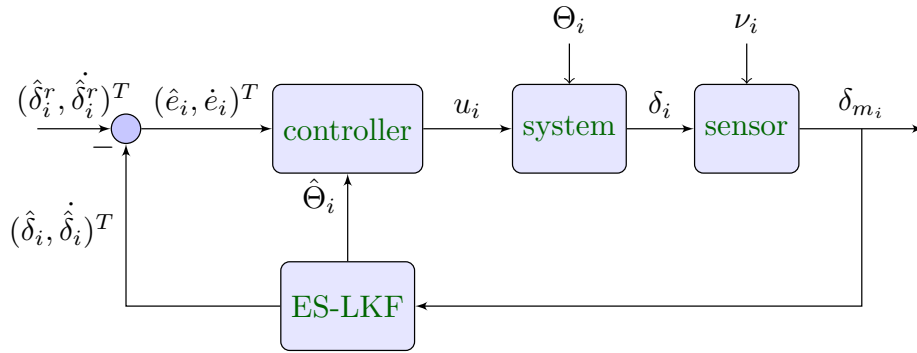


Figure 7: Closed-loop architecture

whose state-space representation is

$$\begin{aligned}\dot{\xi}_1 &= \xi_2 \\ \dot{\xi}_2 &= u^* + \Theta\end{aligned}\tag{38}$$

154 where $\xi_1 = \delta - \delta(t)^d$ and $\xi_2 = \dot{\delta} - \dot{\delta}^d(t)$ are the position and velocity errors, respectively.

156

Remark. For trajectory tracking purposes, i.e. stabilizing the system 158 (Equ.38), requires the full knowledge of the vector state $x = (\delta, \dot{\delta})^T$ and only position is measured. Thus, the state-vector is completed with the LKF-based 160 velocity estimation $\hat{\dot{\delta}}$.

4.2.1. Stability Analysis

162 Before proceeding with the control design, let us present the following useful properties

- 164 • **P1.** $\tanh(\chi) \leq \chi$
- **P2.** $1 \geq \sec^2(\chi) > 0$
- 166 • **P3.** $-\chi < -\tanh(\chi)$
- **P4.** $-\chi^2 < -\tanh^2(\chi)$

where $\chi \in \mathbb{R}^n$. In order to synthesize the controller we use the Backstepping technique. Backstepping starts (stabilizes) with the first integrator (position) by introducing a virtual controller and continue in this sense until reaching the control input at the last step (for details see [21]).

Step 1: Let us propose the Candidate Lyapunov Function (CLF) to deduce a control that provide global asymptotic stability (GAS) for the first integrator subsystem (Equ.38a)

$$\mathcal{V}_1 = \frac{1}{2} \tanh^2(\xi_1)\tag{39}$$

whose the time-derivative

$$\dot{\mathcal{V}}_1 = \tanh(\xi_1)\text{sech}^2(\xi_1)\xi_2 \quad (40)$$

using **P2** (Equ.39) is rewritten as

$$\dot{\mathcal{V}}_1(\xi) \leq \tanh(\xi_1)\xi_2 \quad (41)$$

which is rendered negative-definite ($\dot{\mathcal{V}}_1(\xi) < 0$) provided that

$$\xi_2 = -\lambda_1 \tanh(\xi_1) \quad (42)$$

168 where λ_1 is a positive scalar gain. Hence, we can conclude that ξ_1 is not only stable but also converges asymptotically to the origin.

Step 2: Let us define an error state variable z for ξ_2 , where the previous virtual controller is used as a reference in order to impose a constrained behavior, i.e. $\xi_2^d = -\lambda_1 \tanh(\xi_1)$. Thus, let us consider

$$\tanh(z) \triangleq \xi_2 - \xi_2^d = \xi_2 + \lambda_1 \tanh(\xi_1) \quad (43)$$

from which the state is given

$$\xi_2 = \tanh(z) - \lambda_1 \tanh(\xi_1) \quad (44)$$

Differentiating (Equ.43) yield

$$\text{sech}^2(z)\dot{z} = \dot{\xi}_2 + \text{sech}^2(\xi_1)\dot{\xi}_1 = \dot{\xi}_2 + \text{sech}^2(\xi_1)\lambda_1\xi_2 \quad (45)$$

At this point, using (Equ.44) and (Equ.45), the model (Equ.38)

$$\begin{aligned} \dot{\xi}_1 &= \tanh(z) - \lambda_1 \tanh(\xi_1) \\ \dot{z} &= \frac{1}{\text{sech}^2(z)} [u^* + \Theta + \lambda_1 \text{sech}^2(z)(\tanh(z) - \lambda_1 \tanh(\xi_1))] \end{aligned} \quad (46)$$

Let the final CLF be

$$\mathcal{V}_2 = \frac{1}{2} \tanh(\xi_1)^2 + \frac{1}{2} \tanh^2(z) \quad (47)$$

Obtaining the corresponding time-derivative of $\mathcal{V}_2(\xi_1, z)$ and using **P2** yields

$$\dot{\mathcal{V}}_2 \leq \tanh(\xi_1)\xi_2 + \tanh(z)\dot{z} \quad (48)$$

Using (Equ.46) in (Equ.48) leads to

$$\begin{aligned} \dot{\mathcal{V}}_2 = & \\ & -\lambda_1 \tanh^2(\xi_1) + \tanh(\xi_1) \tanh(z) + \tanh(z) [u^* + \Theta + \lambda_1 \tanh(z) - \lambda_1^2 \tanh(\xi_1)] \end{aligned} \quad (49)$$

In order to render (Equ.49) into a negative-definite function, we introduce the following controller through the error dynamics $\ddot{\xi}$ (Equ. 38b).

$$u^* = -\hat{\Theta} - \tanh(z)(\lambda_1 + \lambda_2), \quad (50)$$

where $\lambda_2 > 0$ is the second gain and also it is considered that δ and $\dot{\delta}$ are origin-convergent states, indicating that after some time τ_1 they lie into the linear domain of $\tanh(\cdot)$. Introducing the controller (Equ. 50) via $\dot{\xi}_2$ (see Equ. 38) in (Equ. 49) leads to

$$\dot{\mathcal{V}}_2 = -\tanh^2(\xi_1) + (1 - \lambda_1^2) \tanh(\xi_1) \tanh(z) - \lambda_2 \tanh^2(z) \quad (51)$$

considering **P3** and **P4** (Equ. 51) is rewritten as

$$\dot{\mathcal{V}}_2 \leq -\xi_1^2 + (1 - \lambda_1^2) \xi_1 z - \lambda_2 z^2 \quad (52)$$

As long as $\lambda_1 > 1$ and $\lambda_2 > 0$, $\dot{\mathcal{V}}_2 \leq 0$ which guarantees stability of the origin and boundedness of the solutions as $t \rightarrow \infty$, i.e.

$$\|(\xi, z)^T\| \leq \gamma, \quad (53)$$

where $\gamma \in \mathbb{R}^+$ stands for the stability region radius. However, we are interested in drawing conclusions about asymptotic stability of the states vector. For this reason, let us consider $\nu = (\xi, z)^T$ and

$$A = \begin{pmatrix} \lambda_1 & -\frac{1-\lambda_1^2}{2} \\ -\frac{1-\lambda_1^2}{2} & \lambda_2 \end{pmatrix} \quad (54)$$

which allows to rewrite (Equ. 52) as

$$\dot{\mathcal{V}}_2 = -\nu^T A \nu \quad (55)$$

¹⁷⁰ which is definite negative if A is positive definite, i.e. $\det[A] > 0$. The latter holds if

- 172 • $\lambda_1^2 > 1$
- $\lambda_2 > \frac{(1-\lambda_1^2)^2}{4\lambda_1}$,

and whose negativity is assured, since the upper bound remains negative, i.e.

$$\dot{\mathcal{V}}_2 \leq -\alpha_{min}\{A\}\|\nu\|^2 \quad (56)$$

174 where $\alpha_{min}\{\cdot\}$ stands for the minimum eigenvalue. Thus, $\dot{\mathcal{V}}_2 < 0$ and hence the
state-vector trajectories converge asymptotically to the origin, i.e. $\xi_1 \rightarrow 0$ and
176 $z \rightarrow 0$, this means that $\xi_2 \rightarrow \tanh(\xi_1)$ fulfilling the tracking objective.

Therefore, replacing (Equ. 50) in (Equ. 35) we obtain the final expression of
the controller written as

$$u = \frac{a}{d_p} \left[-\hat{\Theta} - \tanh(z)(\lambda_1 + \lambda_2) + \ddot{\delta}^d + \tanh\left(\frac{b}{a}\dot{\delta} + \frac{1}{a}\delta\right) \right]$$

5. Numerical results: a comparative study

178 In order to motivate the proposed strategy, we present, for comparative pur-
poses, two control scenarios: the regulation and tracking problems in 1DOF. We
180 observe the disturbance rejection performance of the PID versus the disturbance
compensation based on the ES-LKF. For the actual simulation study we have
182 considered only the hysteresis ($\mathcal{H}(t)$). The parameters used in the simulation
are depicted in table 2.

184 The control integral and ES-LKF-based are described next:

Parameter	value
a_N	0.1×10^{-3}
b_N	0.1×10^{-1}
d_p	4.1083

Table 2: Dynamic parameters of the piezocantilever.

- Since the piezocantilever system (1) features a stable dynamic behavior (natural PD) we add an integral term, with gain $k_i = 10$, activated

$$u = \frac{a}{d_p} \left(\frac{1}{a} \delta^d + \frac{b}{a} \dot{\delta}^d + \ddot{\delta}^d - \frac{k_i}{a} \int_0^t \varepsilon(\tau) d\tau \right) \quad (57)$$

where $\varepsilon = \delta - \delta^d$.

- Next, we have replaced the integral term by the estimation of the disturbance via the ES-LKF.

$$u = \frac{a}{d_p} \left(\frac{1}{a} \delta^d + \frac{b}{a} \dot{\delta}^d + \ddot{\delta}^d + \hat{\mathcal{H}}(t) \right) \quad (58)$$

186 For both cases we activate the control action at $t = 0.75[s]$. Let us consider the following cases:

- 188 1) **Regulation case:** we consider a step sequence reference (frequency= $1[Hz]$ and amplitude= $2[\mu m]$). Thus, the desired position δ^d is a constant reference
190 toggling from $\delta^d = 0[\mu m]$ and $\delta^d = 2[\mu m]$.

Remark. In Fig.8 it is depicted the numerical results where we have noticed
192 that in steady-state the performance that both approaches eliminate the static error. However, within the transitory phase the overshoot smaller with
194 ES-LKF approach. It is noteworthy that bigger values of for integral gain k_i ($k_i > 10$) increase the overshoot and provides a underdamped behavior.

- 196 2) **Trajectory-tracking case:** In this case the objective is to track a time-varying sinusoidal reference (frequency= $1[Hz]$ and amplitude= $2[\mu m]$).

Remark. In Fig.9 it is shown that the compensation effect of both controllers ($t > 7.5[sec]$). The PID controller is not able to compensate, while
200 the controller based on the disturbance estimation tracks the reference trajectory satisfactorily. Moreover, at $t = 1.6[sec]$ it is displayed numerically the
202 deviation between both errors witnessing the effectiveness of the proposed strategy.

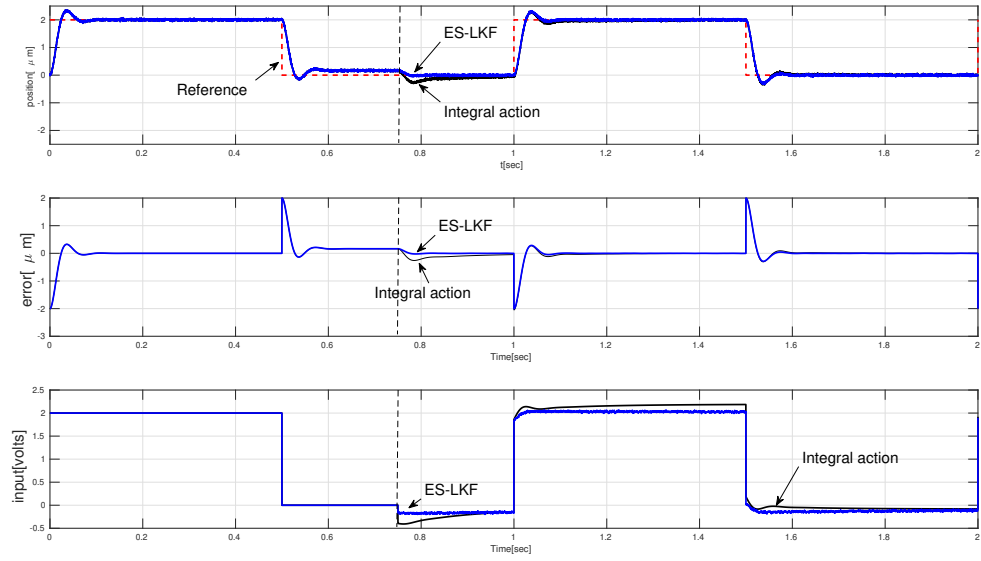


Figure 8: case 1: performance comparison for switching constant reference

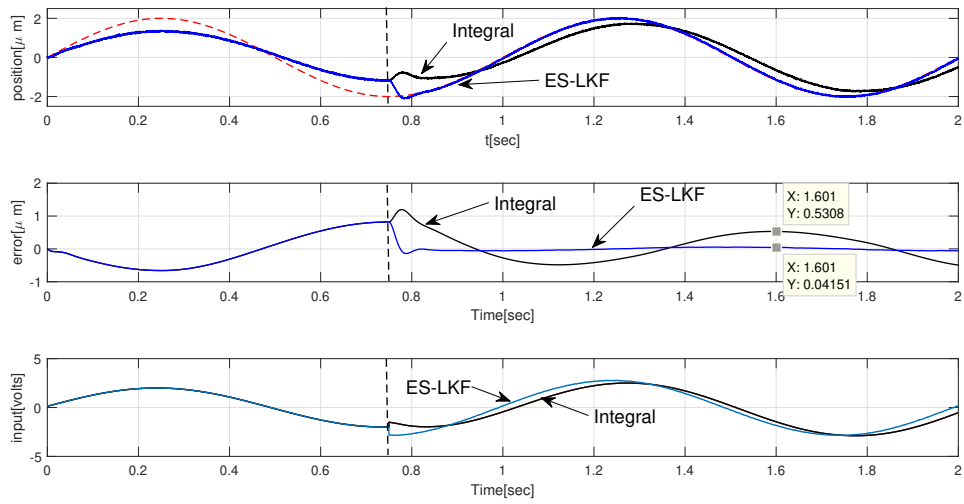


Figure 9: case 2: performance comparison for time-varying sinusoidal reference

204 **6. Real-time Experimental Results**

Section 4 has detailed the estimation strategy of the disturbance (dual-axis hysteresis, couplings and creep) as well as the controller design via a constructive design which guarantees GAS considering the bounded actuators. Therefore, in this section it presented the experimental implementation of the proposed strategy to track circular trajectory for both open- and closed-loop. Indeed, the worst-case scenario occurs during simultaneous 2D positioning generating also cross couplings. The positioning objective is to track a circular pattern at 0.1[Hz] and 1[Hz], and whose expressions are defined by the following time-parametrized functions

$$\begin{aligned} \delta_y(t)^d &= 30 \sin(2\pi ft) \text{ and } \dot{\delta}_y(t)^d = 60\pi f \cos(2\pi ft) \\ \delta_z(t)^d &= 30 \cos(2\pi ft) \text{ and } \dot{\delta}_z(t)^d = -60\pi f \sin(2\pi ft) \end{aligned} \quad (59)$$

206 Firstly, it is presented the open-loop performance to observe the effect of the disturbance on the system's response while attempting to track circular trajectory. Next, the proposed estimation alongside the controller are included to 208 compensate disturbances resulting from tracking a circular trajectory.

Real-time experiments were carried out using Matlab-Simulink[®] which is 210 linked to the dSPACE[®] DAQ¹ via ControlDesk[®]. Experimental parameters are listed on the table 3.

212 *6.1. Open-loop Experiments*

During micro-positioning operations the piezocantilever's performance is significantly deteriorated mainly due to hysteresis and creep. Besides to these adverse effects, multi-DOFs (2DOF in our case) positioning tasks feature internal dynamic couplings, this is shown by the curves matrix in Fig.10 and Fig.11. In the open-loop case we consider a control input including the desired trajectory

¹I/O Acquisition card

Parameter	Value
sampling time T_s	0.2×10^{-3} [sec]
PSD W_{Θ_i}	0.01
R_i	0.04
λ_{1_i}	1.2
λ_{2_i}	1

Table 3: Experimental parameters

without any feedback and/or disturbance estimation, i.e.

$$u = \frac{a}{d_p} \left(\frac{1}{a} \delta^d + \frac{b}{a} \dot{\delta}^d + \ddot{\delta} \right) \quad (60)$$

In Fig. 12 and Fig. 13 it is observed that the error between the reference and the position is quite significant reaching up to 30%. It is witnessed the need of incorporating not only a feedback approach but also disturbance-tolerant trajectory-tracking controllers. On the other hand, the good performance of the position estimation and filtering imply that the overall disturbance $\Theta(t)$ is well estimated. Thus at this stage the ES-LKF estimation is validated.

6.2. Closed-loop Experiments

The experimental stage, presented next, provides a set of results intended to show the effectiveness of the proposed strategy in presence of parametric and parasitic disturbances. Besides the robustness aspect, it is worthwhile highlighting the following:

- The trajectory-tracking objective is performed using the measured position δ_i and estimated velocity.
- The estimation of the lumped disturbance relies fully on the ES-LKF.

The closed-loop scheme illustrated by Fig. 7 is used to compensate the dynamic dual-axis disturbances arising from simultaneous 2D motion (i.e. a

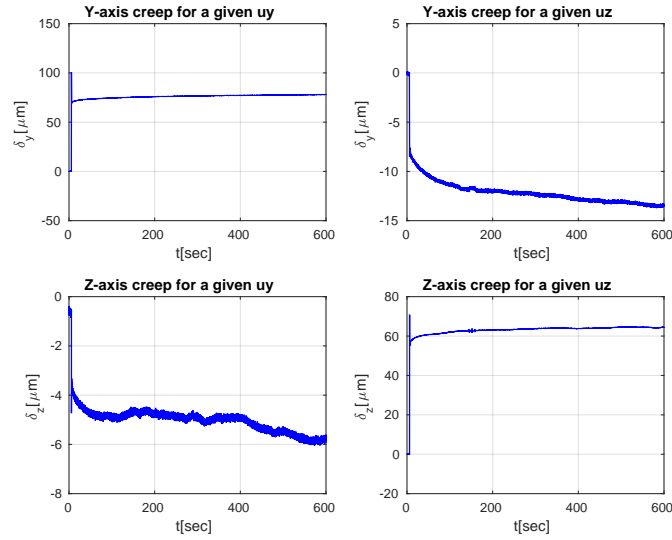


Figure 10: Curves depicting the creep effect and its dual-axis coupling phenomena for an input of 10V in both axes

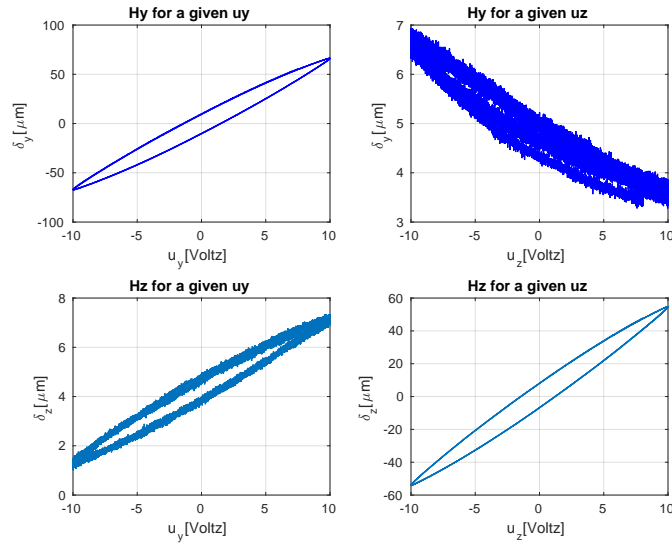


Figure 11: Curves depicting the hysteresis effect and its dual-axis coupling phenomena for a 10V sinusoidal input

circular trajectory reference) with the estimated generalized disturbance $\hat{\Theta}(t)$.

230 In general, experimental results depicted in Fig. 14 and Fig. 15 reveal that

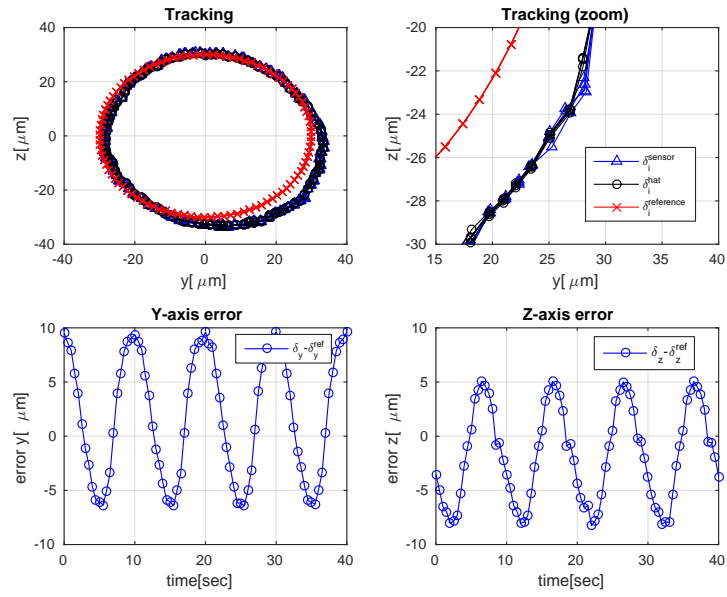


Figure 12: Open-loop performance @ $0.1Hz$

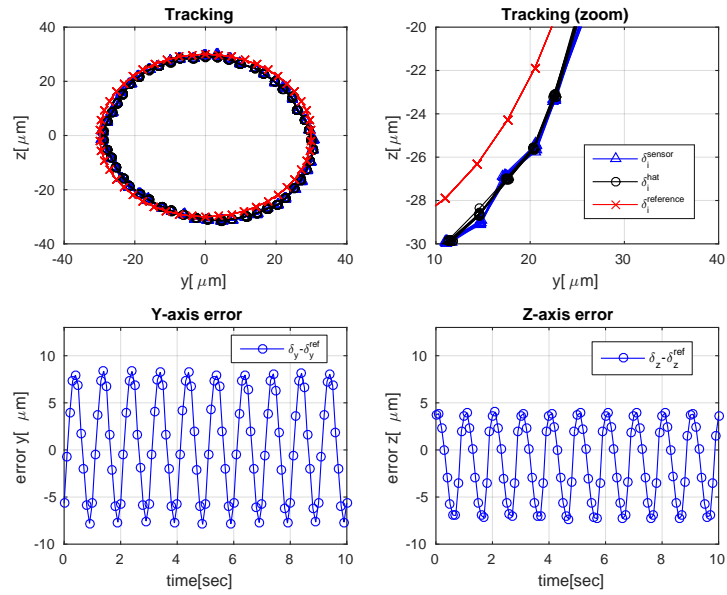


Figure 13: Open-loop performance @ $1Hz$

232 motion objective is fulfilled within the actuator voltage limits. Whereas the
error reached 30% in open-loop, these figures show that the circular reference,
234 at $0.1[Hz]$ and $1[Hz]$, is successfully tracked having errors below 2% for both
axes. It is noteworthy to point out this performance since tracking tasks for
236 second order system requires the knowledge of both states, and therefore the
aforementioned results imply not only the effective estimation of $\hat{\Theta}(t)$ but also
the good velocity estimation considering that only the position measurement is
238 available.

7. Concluding Remarks

240 This paper addressed the control of two degrees of freedom (2-DOF) piezo-
electric actuator (PEA) devoted to micromanipulation tasks. Although the
242 actuator exhibit interesting bandwidth and positioning resolution, it is typified
by strong couplings between its two axes, and strong hysteresis and creep non-
244 linearities. These couplings and nonlinear phenomena finally compromise the
overall performances of the tasks: loss of accuracy, stability compromised.

246 We have witnessed the effectiveness of the proposed estimation-control strat-
egy not only by fulfilling the objective of a dynamic disturbed trajectory-
248 tracking having only position measurement with an estimated velocity, but also
by a successful disturbance ESLKF-based compensation. Moreover, we have
250 shown the flexibility and robustness of the method by presenting two frequency
cases and considering a partial knowledge of the a dynamic model (nominal
252 model). In this paper, we proposed a new strategy to control 2-DOF PEAs for
microrobotics tasks. This strategy is based on two steps : firstly, an estima-
254 tion of the hysteresis, creep and couplings is implemented with a ES-LKF. The
unknown dynamic of this disturbance is simply modeled by a random walk pro-
256 cess (Wiener process). Secondly, this estimation is used in a feedback scheme
to compensate for this disturbance. Extensive experiments were carried out
258 and demonstrate the efficiency of the proposed approach of modeling and control
for low frequency trajectory tracking despite the simplicity of the feedback

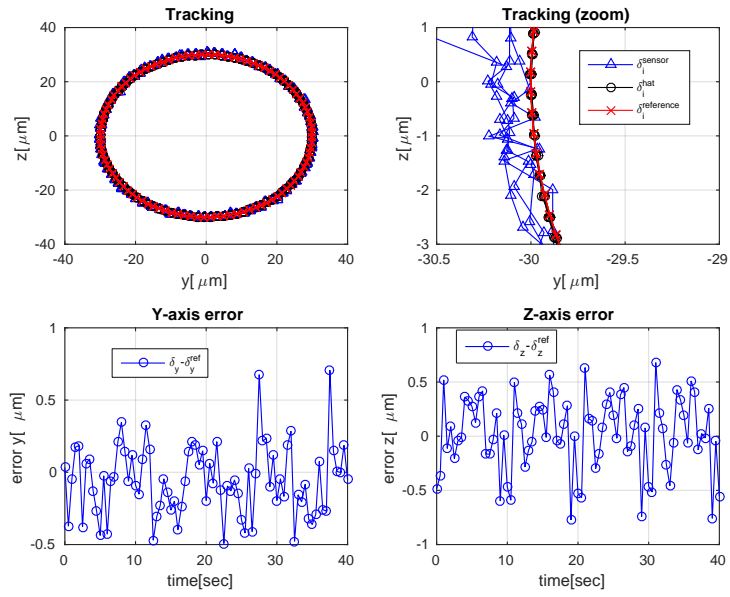


Figure 14: Closed-loop performance @ $0.1Hz$

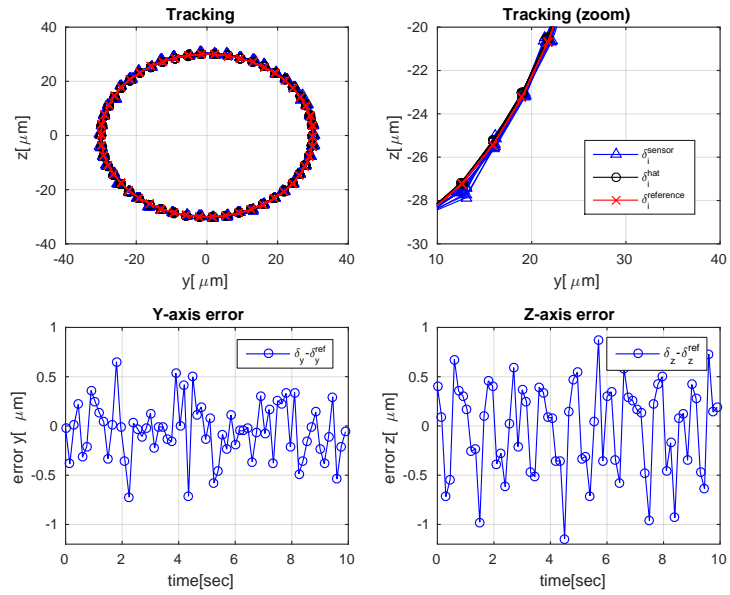


Figure 15: Closed-loop performance @ $1Hz$

260 used. More elaborated control architecture should be developed to deal with
high-speed tracking.

262 **Acknowledgement**

This work was partially supported by the Labex-ACTION (ANR-11-LABX-
264 0001-01). This work was also partially supported by the French Investissements
dAvenir program, project ISITE-BFC (contract ANR-15-IDEX-03).

266 **8. Bibliography**

References

- 268 [1] X. T. R.V. Iyer, P. Krishnaprasad, Approximate inversion of the preisach
hysteresis operator with application to control of smart actuators, IEEE
270 Transactions on Automatic Control 50 (6).
- [2] G. S. D. Croft, S. Devasia, Creep, hysteresis and vibration compensation
272 for piezoactuators: atomic force microscopy application, ASME Journal of
Dynamic Systems, Measurement and Control 123 (50).
- 274 [3] J. M. A. Dubra, C. Paterson, Preisach classical and nonlinear modeling of
hysteresis in piezoceramic deformable mirrors, Optics Express 13 (22).
- 276 [4] M. Rakotondrabe, Multivariable classical prandtl-ishlinskii hysteresis
modeling and compensation and sensorless control of a nonlinear 2-
278 dof piezoactuator, Springer Nonlinear Dynamics (NODY)doi:10.1007/
s11071-017-3466-5.
- 280 [5] B. Mokaberi, A. A. G. Requicha, Compensation of scanner creep and hys-
teresis for afm nanomanipulation, IEEE Transactions on Automation Sci-
282 ence and Engineering 5 (2).
- [6] M. Rakotondrabe, Classical prandtl-ishlinskii modeling and inverse multi-
284 plicative structure to compensate hysteresis in piezoactuators, American
Control Conference.

- 286 [7] M. A. Janaideh, P. Krejci, Inverse rate-dependent prandtl-ishlinskii model
for feedforward compensation of hysteresis in a piezomicropositioning ac-
288 tuator, *IEEE/ASME Transactions on Mechatronics* 18 (5).
- [8] M. Rakotondrabe, Bouc-wen modeling and inverse multiplicative struc-
290 ture to compensate hysteresis nonlinearity in piezoelectric actuators, *IEEE
Transactions on Automation Science and Engineering* 8 (2).
- 292 [9] M. R. Didace Habineza, Y. L. Gorrec, Bouc-wen modeling and feedforward
control of multivariable hysteresis in piezoelectric systems: Application to
294 a 3-dof piezotube scanner, *IEEE Transactions on Control Systems Tech-
nology* DOI.10.1109/TCST.2014.2386779.
- 296 [10] F.-J. Lin, H.-J. Shieh, P.-K. Huang, L.-T. Teng, Adaptive control with
hysteresis estimation and compensation using rfnn for piezo-actuator, *Ul-
298 trasonics, Ferroelectrics, and Frequency Control*, *IEEE Transactions on
53* (9) (2006) 1649–1661. doi:10.1109/TUFFC.2006.1678193.
- 300 [11] F.-J. Lin, H.-J. Shieh, P.-K. Huang, Adaptive wavelet neural network con-
trol with hysteresis estimation for piezo-positioning mechanism, *Neural
302 Networks*, *IEEE Transactions on* 17 (2) (2006) 432–444. doi:10.1109/
TNN.2005.863473.
- 304 [12] Y. Li, Q. Xu, Adaptive sliding mode control with perturbation estimation
and pid sliding surface for motion tracking of a piezo-driven micromanip-
306 ulator, *Control Systems Technology*, *IEEE Transactions on* 18 (4) (2010)
798–810. doi:10.1109/TCST.2009.2028878.
- 308 [13] X. Chen, T. Hisayama, Adaptive sliding-mode position control for piezo-
actuated stage, *Industrial Electronics*, *IEEE Transactions on* 55 (11) (2008)
310 3927–3934. doi:10.1109/TIE.2008.926768.
- [14] M. V. S. A. Sebastian, J. P. Cleveland, Robust control approach to atomic
312 force microscopy, *Conference on Decision and Control*.

- [15] Y. H. Micky Rakotondrabe, P. Lutz, Plurilinear modeling and discrete mu-
314 synthesis control of a hysteretic and creeped unimorph piezoelectric can-
tilever, IEEE International Conference on Automation, Robotics, Control
316 and Vision.
- [16] M. R. Sofiane Khadraoui, P. Lutz, Combining h-inf approach and interval
318 tools to design a low order and robust controller for systems with parametric
uncertainties: application to piezoelectric actuators, International Journal
320 of Control 85 (3).
- [17] M. Boudaoud, Y. Haddab, Y. Le Gorrec, Modeling and optimal force con-
322 trol of a nonlinear electrostatic microgripper, Mechatronics, IEEE/ASME
Transactions on 18 (3) (2013) 1130–1139. doi:10.1109/TMECH.2012.
324 2197216.
- [18] M. Rakotondrabe, P. Lutz, Force estimation in a piezoelectric cantilever
326 using the inverse-dynamics-based uio technique, in: Robotics and Automa-
tion, 2009. ICRA '09. IEEE International Conference on, 2009, pp. 2205–
328 2210. doi:10.1109/ROBOT.2009.5152178.
- [19] E. Piat, J. Abadie, S. Oster, Nanoforce estimation with kalman filtering
330 applied to a force sensor based on diamagnetic levitation, in: Intelligent
Robots and Systems (IROS), 2011 IEEE/RSJ International Conference on,
332 2011, pp. 39–44. doi:10.1109/IROS.2011.6094457.
- [20] A. J. Fleming, A review of nanometer resolution position sensors: Opera-
334 tion and performance, Sensors and Actuators A: Physical 190 (2013) 106 –
126. doi:https://doi.org/10.1016/j.sna.2012.10.016".
- [21] R. Sepulchre, M. Janković, P. Kokotović, Constructive Nonlinear Control,
336 Communications and control engineering, W.H. Freeman., 1997.
338 URL <https://books.google.fr/books?id=JKIeAQAAIAAJ>